Inorganic Chemistry Communications 152 (2023) 110648

Contents lists available at ScienceDirect

Inorganic Chemistry Communications

journal homepage: www.elsevier.com/locate/inoche

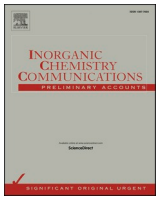

Short communication

Preparation and characterization of new optical active charge transfer complexes for mitigation climate changes

Mervette. El Batouti [a], E.H. El-Mossalamy [b], H.A. Fetouh [a,*]

[a] Chemistry Department, Faculty of Science, Alexandria University, Egypt
[b] Chemistry Department, Faculty of Science, Benha University, Egypt

ARTICLE INFO

Keywords:
Schiff base
Charge transfer complexes
Climate change
IR absorption
Thermal Conductivity

ABSTRACT

The background of this work is based on preparation and characterization of new optically active charge transfer complexes (CTC) to harvest weak infra-red photons emitted from sun light to avoid thermal heat and converting such waste heat into useful work. The innovation in study is that it is first time to prepare such new that absorb in IR and have good thermal conductivity. The obtained results have good impact in both material science and academic research. Electron-donors thiophene Schiff bases: 2-((2-OH-benzylidene) amino) −4, 5, 6, 7-tetrahydrobenzo[b] thiophene-3-carbonitrile (D1) and 2-((Furan-2ylmethylene) amino) 4, 5, 6, 7 tetrahydrobenzo[b] thiophene-3-carbonitrile (D2) are prepared. For the first time as novelty, these electron donors Schiff bases are intercalated to electron-acceptor picric acid (A1) derivative (A2) forming new charge transfer complexes (CTC). Low charge transfer energy in the range 2.899 eV-3.316 eV reflects good non linear optical activity. Molar extinction coefficients (ϵ, $M^{-1}cm^{-1} \times 10^3$) CTC [(D1) (A2)2], [(D2) (A2)], [(D2) (A2)2] are 125.6, 129.9, and 133.41 respectively reflect excellent optical activities. Deposition CTC as thin film (TF) aluminium foil decrease energy gap of [D1A1] and enhanced absorption of thermal energy of weak IR photons. High thermal conductivity of CTC ranging from 1.1 $W.min^{-1}.K^{-1}$ to 1.6 $W.min^{-1}.K^{-1}$ for different particle size. This behavior enabled attenuation of electromagnetic radiation and rapid heat dissipation due to dielectric properties and polarity. On heating, AC electrical conductivity of CTC and dielectric properties confirmed attenuation of thermal infra-red radiation results from golbal warming results from climate change in hot summer season.

1. Introduction

Using advanced new optically active materials improved human life by providing more practical various devices and facilities such as efficient photo catalytic degradation of: toxic organic and environmental contaminants, organic solar cells, desalination of salt water [1–3]; manufacture of photo detectors [4,5]; fabrications of fluorescence emission sensors for toxic pollutants such as carbon dioxide [6,7]. Fourier transform infrared (FTIR) spectroscopy is used for qualitative and some quantitative analysis of IR active material that showed none zero dipole moment on absorption of IR photon.

IR spectra is a fingerprint of a sample with vibrational absorption peaks corresponding to vibrational frequencies of atomic bonds. FTIR overcome limitations in dispersive instruments [8]. However, slow scanning process retard simultaneous measuring of all IR vibrational frequencies [8].This problem is solved *via* employing CTC in IR spectrophotometer to produces unique signals of all encoded IR frequencies [9]. Signal can be measured quickly at one *sec* per sample and FTIR spectroscopy becomes rapid, sensitive.[10].

CTC of Schiff bases are used in pharmacy and medicine as antibacterial, antifungal and antiviral [11].Charge-transfer interaction between electron-donor (es-donor) and electron-acceptor (es-acceptor) clarifies both therapeutic drug-receptor interactions, in vivo drug releases [12] and drug-receptor interactions and medication mechanism in biological fluids. CTC 2, 2′-bipyridine-picric acid (PA) and chloranilic acid 1:1 stoichiometry formed *via* H^+ migration from es-acceptor to es-donor followed by intra-molecular hydrogen bonds (HB) [13]. Formation constants (K_f) of CTC depend on structure of es-acceptors [13]. *CT* complexation is enhanced on es transfer from es-donor such as phenothiazine from excited state to es-acceptor with low lying lowest unoccupied molecular orbital (LUMO)[14].

CTC of Schiff bases are widely used in pharmaceuticals and chemotherapeutic drug formulations [13]. Biological (antibacterial, antifungal and antiviral) activity of CTC is much higher than that of es-donor and

* Corresponding author.
E-mail addresses: mervette_b@yahoo.com (Mervette. El Batouti), howida_fetouh@alexu.edu.eg (H.A. Fetouh).

https://doi.org/10.1016/j.inoche.2023.110648
Received 2 December 2022; Received in revised form 11 March 2023; Accepted 22 March 2023
Available online 28 March 2023

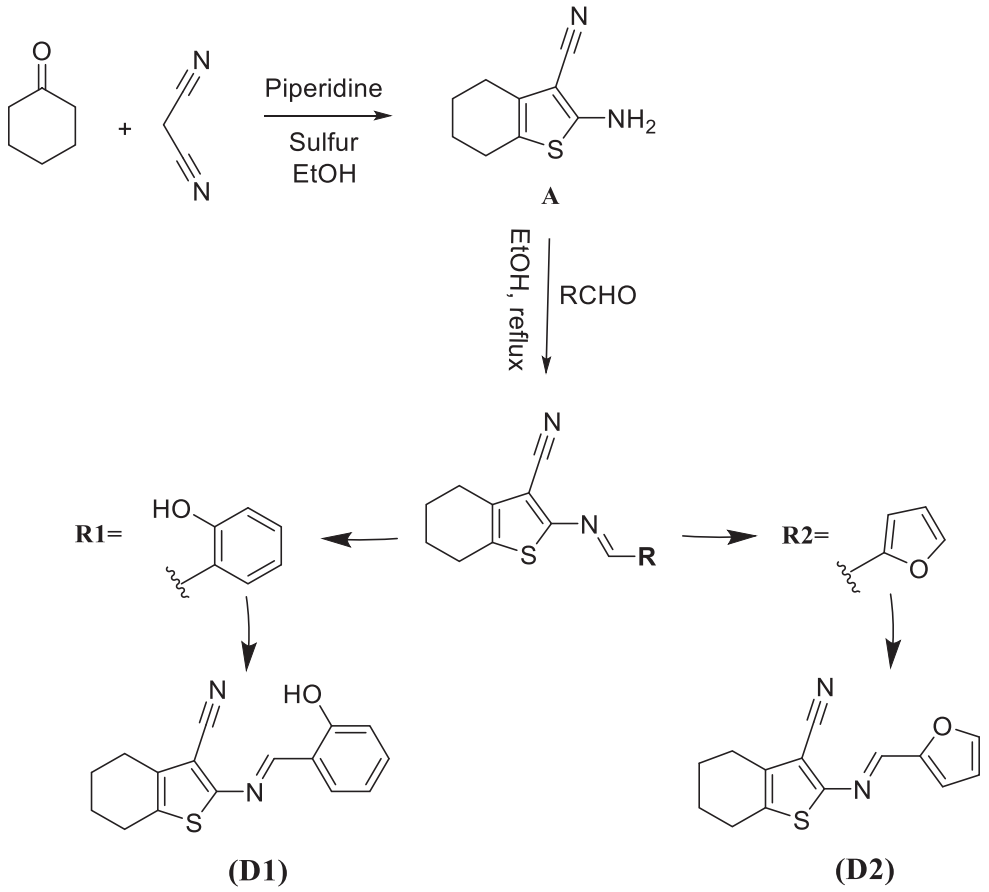

Scheme 1. Synthesis of Schiff bases D1, D2 [18].

es-acceptor components. Biological cell membrane acts as an electrode where bio-electrochemical reactions and biological processes occurs such as replication of macromolecules or generation of biological ''motors" [17]. CTC are used in medicine and pharmacology due to antimicrobial activity. Biocide activity of CTC enables their uses as biomarkers for microorganisms in polluted wastewater contain high abundant organic matters. In vivo interaction and replication of plasmid bacterial DNA with adsorbed es-donor material gives CTC on adrenergic receptor (has intact or native conformation) sites at cell membrane. These CTC prevents competitive accumulation of possible metabolites with plasmid DNA replication [18]. Biological activity of CTC 2, 6-diaminopyridine-PA depends on molecular structure [11]. Positively charged CTC: phenytoin-2, 6-di-Cl- -quinone-4-Cl-imide; 2, 6-di-Br-quinone-4-Cl-imide, *N*-Br-succinimide, streptomycin physically adsorbed on bacterial cell membrane causing pitting [19].

Sun providing thousands ($W.m^{-2}$) thermal power energy daily on earth surface. Total solar energy in upper atmosphere contains 50 % IR radiation, 40 % Vis. light and 10 % UV radiation. IR radiation causes vibration transition heats earth's surface [15]. Attenuation of thermal energy can be achieved by painting glass windows by CTC filtering and rapidly dissipate IR radiation. High thermal conductivity of optically active CTC is a prerequisite for rapid attenuation of incident IR electromagnetic radiation by dielectric components IR, converted into waste heat into useful work [16]. Various CTC are prepared [17,20–23].

This study aims to prepare and characterize new optically active CTC of thiophene Schiff bases with es-acceptor picric acid and its derivative. Their chemical structure will be tuned to absorb thermal energy of weak IR photons to mitigate thermal energy caused climate changes.

2. Methods and materials

All chemicals used in this study have high purity of analytical grades are purchased from Sigma Aldrich Co. (Except: PA (purity, 99.5 %) and its derivative 2, 4-di-NO_2-phenol 85 % purity from Merck Co., Germany) used as received without further purification. Thiophene Schiff bases D1, D2 are prepared as described elsewhere [18]. Piperidine (purity 99 % (0.85 g, 10 mmol) is slowly added to: 2.94 g, 30 mmol cyclohexane, malononitrile (purity, 99 %, 1.32 g, 20 mmol) and sulfur element (purity, 99.99, 0.64 g, 20 mmol) in 20 mL EtOH, 50 °C. Reaction mixture is heated refluxed for 2 h., left overnight for cooling. Precipitate is filtered and washed with 20 mL cold ethanol forming (compound **A**: 0.89 g, 5 mmol) is dissolved in ethanol. An equimolar amount of corresponding aldehyde (R1 phenol, R_2 furan) is added drop wise, Scheme 1. Mixture is stirred at room temperature till product crashed out of solvent as precipitate. Reaction mixture is agitated further till detection reaction completion using TLC. Product was filtered off and washed with 2 × 5 mL cold ethanol and recrystallized from hot [18].

Physical properties of D1, D2 are recorded in supplementary information (SI), Table SI.1.

For the first time, the novelty of this study involved preparation of CTC thiophene- PA. Stoichiometry 1:1 M ratio-solid CTC are prepared by mixing equi-molar concentration D1, D2 (50 mL ethanol) with A1 or A2 (10 mL ethanol); stirring 20 min., slow evaporation at room temperature and filtration. Solid CTC are washed with methanol, collected and dried under vacuum over anhydrous $CaCl_2$ for 24 h. CTC [(D1) (A1)], [(D1) (A2)], [(D2) (A1)] and [(D2) (A2)] are crystallized from ethanol.

CTC in 1:2 [(D1) $(A1)_2$], [(D1)$(A2)_2$], [(D2)$(A1)_2$] and [(D2)$(A2)_2$] are prepared by mixing 1 mmol. D1 or D2) (50 mL ethanol solution) with 2 mmoL. A1 or A2 (10 mL ethanol) then followed the same procedure in

Table 1
Representative analytical and physicochemical data of CTC.

Stoichiometric ratio	Reactants (mmol, g)	Molecular Formula, Mw. g.mol.$^{-1}$	m.p. °C	Color	Elemental analysis; observed/calc.		
					%C	%H	%N
[(D1)(A1)] 1:1	D1: A1(1, 0.282): (1, 0.229)	$C_{22}H_{17}N_5O_8S$ 511	152	Yellow	50.26/51.66	3.12/3.35	13.88/13.69
[(D1)(A1)$_2$] 1:2	D1: 2 A1(1, 0.282): (2, 0.458)	$C_{28}H_{20}N_8O_{15}S$ 740	72	Brown	44.87/45.41	2.91/2.72	14.75/15.13
[(D1)(A2)] 1:1	D1: A2(1, 0.282): (1, 0.184)	$C_{22}H_{18}N_4O_6S$ 466	170	Pale yellow	57.34/56.65	3.65/3.89	11.82/12.01
[(D1)(A2)$_2$] 1:2	D1: 2 A2(1, 0.282): (2, 0.368)	$C_{28}H_{22}N_6O_{11}S$ 650	98	Yellow	52.07/51.69	3.52/3.41	12.78/12.92

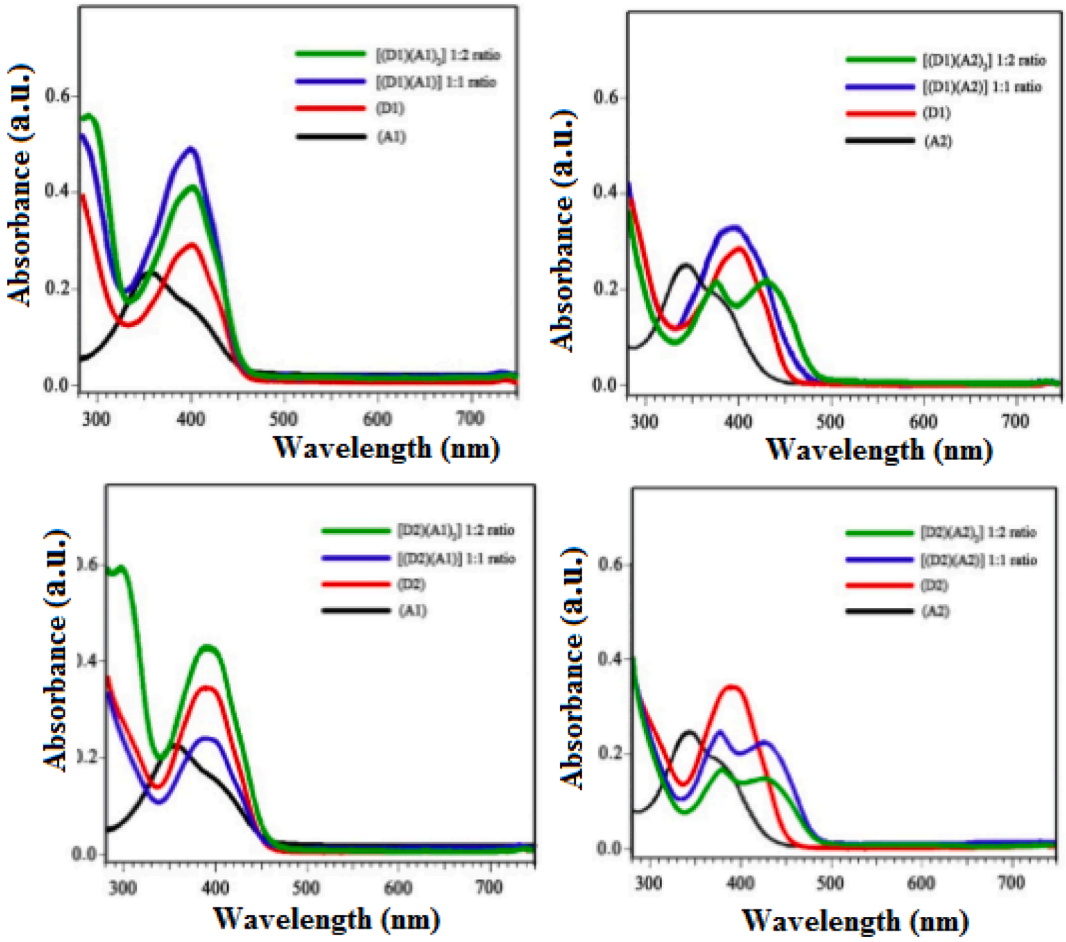

Fig. 1. UV–vis. electronic absorption bands.

preparation 1:1 CTC [18].

The compounds D1, D2 and CTC are characterized by elemental analysis; m.p.; UV–vis absorption and vibration IR spectroscopy in ethanol at 25 °C using Perkin-Elmer 1430 Buck scientific 500-IR spectrophotometer. 1.0 mg sample is fine grinded with excess KBr powder. Mixture is compressed under 10 k bar pressure giving clear transparent disc. Mass spectra (MS) are recorded on a direct probe controller inlet part to single quadrat pole Thermos Scientific GC–MS analyzer, model ISQ LT using Thermo X-Calibur software. Electronic absorption spectra at 200–800 nm; 1.0 cm quartz cells, JASCO V-530 UV–vis. Spectrophotometer [18].

3. Results and discussion

Elemental analysis showed stoichiometry of CTC (donor: acceptor molar ratio) is either1:1 or 1:2, together with m.p. confirmed molecular structures, Table 1.

Both m.p. represent (energy required for melting solid CTC attaining solid–liquid equilibrium confirmed CTC [(D1) (A2)] has the most physically stable solid phase having good crystallinity. Both observed and calculated elemental analysis agreed well [18].

MS, Fig. SI.1.and fragmentation patterns and the last ionized fragment confirmed molecular weight (Mw.) of D1 282 g.mol.$^{-1}$, and D2 256 g.mol.$^{-1}$ For D1, fragment ion peaks are caused by bond cleavage at different positions. Common fragmentations give various observed base peaks at *m/z* ratio correspond to molecular ion peak; $[C_{16}H_{14}N_2OS]^+$, $[C_{15}H_{11}N_2S]^+$, $[C_6H_5O]^+$, $[C_6H_4]^+$, $[C_4H_8]^+$, $[C_4H_3]^+$, $[C_2H_2O]^+$ ions. Fragmentation pattern yield $[C_{14}H_{12}N_2OS$, $[C_2H_2N]^+$, $[C_{12}H_8N_2OS]^+$ from cleavage cyclohexane ring, $[C_5NS]^+$, $[C_2H_2O]^+$, $[C_4H_3]^+$, $[C_4H_8]^+$ and $[C_2H_2O]^+ + 2H^\bullet$ fragments [19].

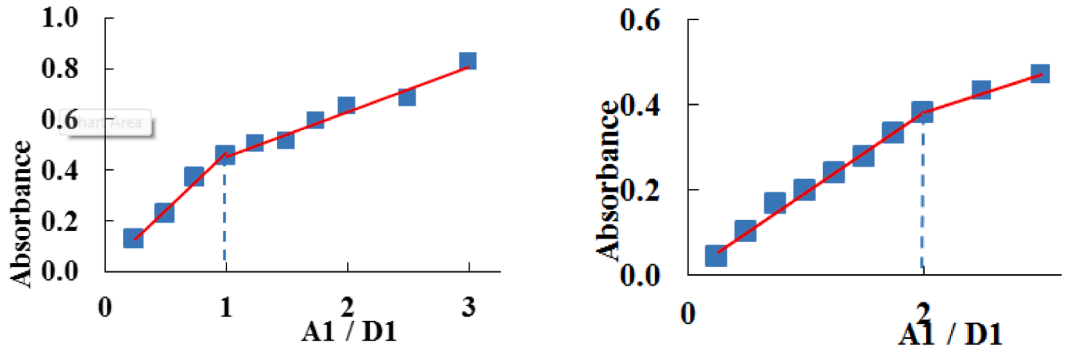

(a): [(D1)(A1)]at 395 nm (b): [(D1)(A1)$_2$] at 398 nm

Fig. 2. Represntative photometric titration curve of CTC in ethanol.

Table 2
Characteristic IR frequencies* (cm^{-1}) and tentative assignments.

(D1)	(A1)	[(D1)(A1)]	[(D1)(A1)$_2$]	Assignments
3426 s,br	3416 s,br	3442 s,br	3438 s,br	ν (O — H)
3050 w	3103 *m*	3058 w	3060 w	ν (C — H)$_{ar}$
2218 s		2217 s	2218 s	ν (C≡N)
1599 vs		1601 vs	1604 s	ν (C═N)
	1607 s	1561 m	1560 m	ν_{as} (NO_2)
1442 s		1442 s	1442 s	δ_{ip}(O — H)
	1312 s	1325 w	1326 w	ν_s (NO_2)
1279 s		1276 m	1276 m	δ (O — H)
756 vs	732 s	767 s	768 s	δ_{oop} (C — H)$_{ar}$
686 w		683 w	697 w	ν (C — S)
	522 m	526 w	527 w	δ (ONO)
D1	A2	[(D1)(A2)]	[(D1)(A2)$_2$]	
3426 s,br	3374 m,br	3443 s,br	3428 s,br	ν (O — H)
3050 w	3109 w	3065 w	3067 w	ν (C — H)$_{ar}$
2218 s		2218 s	2217 s	ν (C≡N)
1599 vs		1600 vs	1600 s	ν (C═N)
	1517 s	1484 m	1478 m	ν_{as} (NO_2)
1442 s	1433 s	1438 s	1436 s	δ_{ip}(O — H)
	1347 s	1339 s	1336 s	ν_s (NO_2)
1279 s	1270 m	1276 m	1273 m	δ (O — H)
780 s		773 m	770 m	δ_{oop} (CH_2)
756 vs		756 s	756 s	δ_{oop} (C — H)$_{ar}$
686 w		683 w	684 w	ν (C — S)
574	524 w	526 w	525 w	δ (ONO)

* s: strong, m: medium, w: weak, br: broad, v: very, ip: in-plane, oop: out-of-plane, *ν*: stretch, δ: bending, ar: aromatic ring.

Vibrational IR spectra, Fig. SI.2 identified functional groups [27] in CTC, Fig. 2. Assigned characterized vibrational bands are given in Table 2. D1A1 has intense vibrational IR bands. Donor and acceptors in CTC revealed small shifts in wavenumber ($\overline{\nu}$) and intensities compared with free Ds and As. *CTC* showed absorption bands at 3600–2450 cm^{-1} of free D.

Main interaction occurs *via* H^+- and electron transfer between Ds and As. IR spectra of CTC changed on complexation. C — H bands of D shifted to $\bar{\nu}$. Those of A shifted to lower $\bar{\nu}$ by π-π* CT interaction, ν (C — H) at 3050 in D1 cm^{-1} shifted to 3058 cm^{-1} and 3060 cm^{-1} for [(D1)(A1)] and [(D1) (A1) $_2$] respectively. H^+ transfer from phenolic OH groups of PA to basic center of donor molecule masked OH-band of A and shifted $\nu_{C=N}$ band to 1601 cm^{-1} and 1604 cm^{-1} for [(D1)(A1)] and [(D1)(A1)$_2$] respectively [20].

Dipoles caused by semipolar N → O bond alter band position, especially anti-symmetric stretching, vibration ν_{as} (NO_2) sensitive for polar influences and electronic states of nucleus. Hence, shift to $\bar{\nu}$ $_{as}$(NO_2) vibration (1561, 1560 cm^{-1}) in CTC compared with A1 (1607 cm^{-1}) due to increased electron density on picrate unit on CT interaction. H^+ transfer from PA to D [18].

Vibrational IR spectra clarified functional groups characterizing CTC and confirm molecular structure. Bands of CTC are blue shifted $\bar{\nu}$ and more intense than Ds and As. Interaction involving H^+ transfer and eT when D(s) react with acidic A(s). C — H bands of Ds shifted to high $\bar{\nu}$ and those of A(s) shifted to lower $\bar{\nu}$ due to π-π* CT interaction, $\nu_{(C—H)}$ at 3050 shifted to 3058 cm^{-1} and 3060 cm^{-1} in D1 and [(D1)(A1)$_2$] respectively. H^+ transfer from phenol basic OH groups of PA disappeared OH band of A, $\nu_{C=N}$ shifted to high $\bar{\nu}$ 1601 cm^{-1+}, 1604 cm^{-1} for [(D1)(A1)], [(D1)

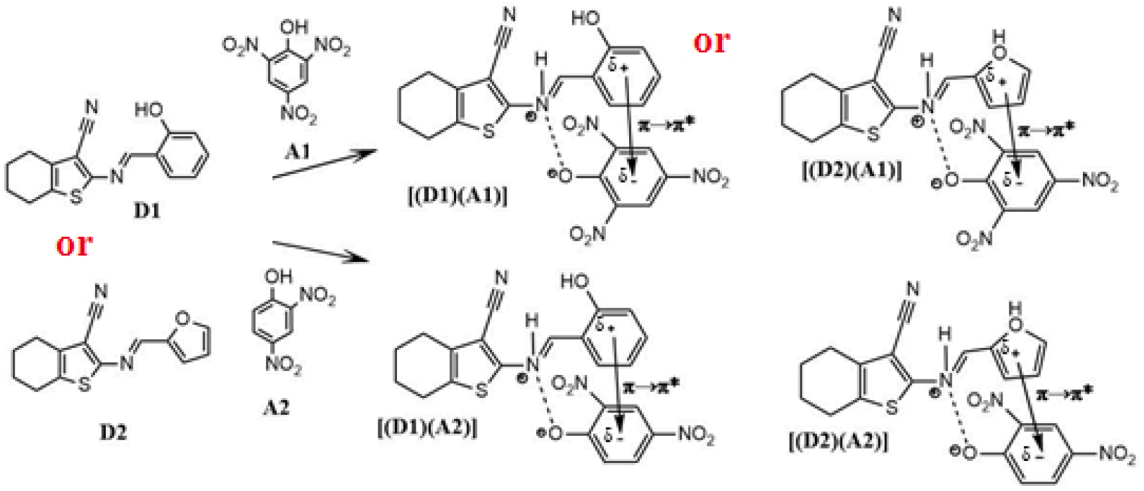

Scheme 2. Proposed CTC of D1, D2 with A1, A2 1:1 M stoichiometric ratio.

Table 3
Values of $C^{\circ}_d \cdot C^{\circ}_a/A, C^{\circ}_d + C^{\circ}_a$

$C^{\circ}_a \times 10^{-4}$	$C^{\circ}_d \times 10^{-4}$	Ratio (a/d)	$C^{\circ}_d + C^{\circ}_a \times 10^{-4}$	$C^{\circ}_d \cdot C^{\circ}_a \times 10^{-8}$	1:1[(D1)(A1)]		1:2[(D1)(A1)$_2$]	
					A 395 nm	$C^{\circ}_d \cdot C^{\circ}_a/A \times 10^{-8}$	A 398 nm	$C^{\circ}_d \cdot C^{\circ}_a/A \times 10^{-8}$
0.25	1.00	0.25	1.25	0.25	0.129	1.943	0.044	5.656
0.50	1.00	0.50	1.50	0.50	0.229	2.185	0.101	4.931
0.75	1.00	0.75	1.75	0.75	0.369	2.031	0.168	4.472
1.00	1.00	1.00	2.00	1.00	0.456	2.192	0.198	5.061
1.25	1.00	1.25	2.25	1.25	0.501	2.498	0.239	5.226
1.50	1.00	1.50	2.50	1.50	0.512	2.929	0.280	5.367
2.00	1.00	2.00	3.50	2.50	0.647	3.862	0.382	6.541
2.50	1.00	2.50	4.00	3.00	0.680	4.412	0.432	6.951
3.00	1.00	3.00	4.50	3.50	0.822	4.260	0.469	7.458

					1:1 [(D1)(A2)]		1:2 [(D1)(A2)$_2$]			
					397 nm	$\times 10^{-8}$	375 nm	$\times 10^{-8}$	429 nm	$\times 10^{-8}$
0.25	1.00	0.25	1.25	0.25	0.153	1.631	0.087	2.877	0.098	2.554
0.50	1.00	0.50	1.50	0.50	0.212	2.357	0.110	4.545	0.142	3.524
0.75	1.00	0.75	1.75	0.75	0.319	2.350	0.147	5.088	0.177	4.235
1.00	1.00	1.00	2.00	1.00	0.385	2.595	0.168	5.942	0.213	4.686
1.25	1.00	1.25	2.25	1.25	0.411	3.045	0.202	6.176	0.245	5.096
1.50	1.00	1.50	2.50	1.50	0.401	3.740	0.219	6.852	0.276	5.433
2.00	1.00	2.00	3.50	2.50	0.439	5.696	0.261	9.590	0.341	7.331
2.50	1.00	2.50	4.00	3.00	0.443	6.770	0.265	11.316	0.353	8.496
3.00	1.00	3.00	4.50	3.50	0.445	7.862	0.277	12.626	0.362	9.671

(A1)$_2$] respectively. Dipole caused by semi polar N → O bond makes band position, especially anti-symmetric stretching, ν_{asNO2} sensitive for polarity and electronic and nuclear states: shift to low $\overline{\upsilon}_{NO2}$ (1561, 1560 cm^{-1}) in [(D1)(A2)], [(D1) (A2)$_2$] respectively compared with A1 (1607 cm^{-1}) in the same manner as [(D1)(A1)], [(D1) (A1) $_2$]. Shifts $\overline{\upsilon}_{C-H}$ of D indicat that aromatic rings are interaction center. Asymmetric NO_2-bands of Asas appeared two adjacent peaks. Lower energy bands shifted to low $\overline{\upsilon}$indicating strongly polarized NO_2-groups by high electron density on aromatic ring of A. An asymmetric NO_2 - band of CTC with A2 shifted to low $\overline{\upsilon}$ and n–π* interaction is excluded. Shift of IR spectra of CTC with (A2): asymmetric NO_2-band at 1517 cm^{-1} for A shifted to low $\overline{\upsilon}$ 1484 cm^{-1}, 1478 cm^{-1} for [(D1)(A2)], [(D1)(A2)$_2$]. Symmetric $\nu_{s\ NO2}$ band at 1347 cm^{-1} shifted to 1339 cm^{-1}, 1336 cm^{-1} for CTC, ν_{O-H} peak in CTC shifted from D1, 3426 cm^{-1}, (A2, 3374 cm^{-1}) to 3443 cm^{-1}, 3428 cm^{-1} in [(D1)(A2)] and [(D1)(A2)$_2$] respectively [21].

^{1}H NMR spectra, Fig. SI.3 showed comparative study among all tested samples. In CTC, ^{1}H NMR signals shifted to lower field of Ds and As. Higher frequency shift occurs as ππ* interaction increased π-es density on As and decrease on D. Shift magnitude varies from D to A; shift is higher with signals due to phenol ring H^+ in accordance with IR spectra. [(D1)(A1)] and [(D1)(A1)$_2$] exhibited new signal at 6.5 ppm and 6.4 ppm due to (CH = N^+ - H) proton. Downfield shift of signals correspond to proton of cyclohexane ring is caused by deshielding effect of positive hole left on phenol ring after CT interaction. [(D1)(A2)] and [(D1)(A2)$_2$] exhibited new signal at 8.4 ppm and 8.6 ppm (CH = N^+ - H). Downfield shifts of signals correspond to H^+ of cyclohexane ring is caused by deshielding effect of positive hole left on phenol ring after CT interaction [18]. Functional group CH = N^+ - H and multiple oxygen atoms in CTC enhanced intercalation on aluminium foil [22].

Donors-acceptors interaction 1:1, 1:2 M ratio are represented by Scheme 2 [18]].

Electronic UV–vis. absorption spectra of D1 and *CTC* are shown in Fig. 1. Small shift on absorption band of free donor spectra attributed to *CT*-interactions at 397 nm with CT energy, ECT 3.132 eV for [(D1) (A2)]. [(D1) (A2)$_2$], observed two bands at 375 nm, 429 nm with E_{CT} 3.316 eV, 2.899 eV respectively [18].

CTC absorb incident UV–vis. photon from sun light generating e-hole pair and current flow depending on photon energy. CT band 365–430 nm corresponds to intermolecular CT interaction, E_{CT} 3.41–2.88 eV. Band shift of A at 360 nm and small shift on band in D at 400 nm to 395 nm, E_{CT} 3.149 eV and 398 nm with E_{CT} 3.125 eV for [(D1)(A1)] and [(D1)(A1)$_2$] respectively are due to *CT*-interactions. PA acidity is due to

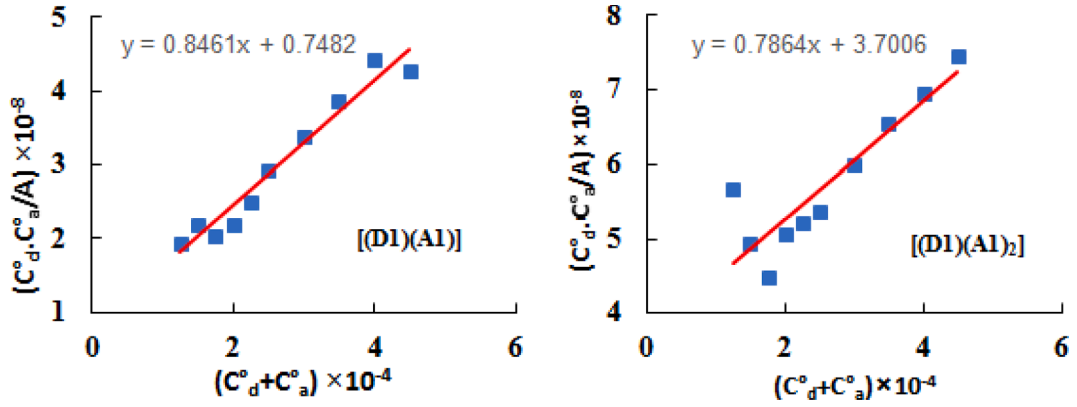

Fig. 3. Relation between $C^{\circ}_d \cdot C^{\circ}_a/A$ and $C^{\circ}_d + C^{\circ}_a$ for CTC.

Table 4
Comparison of reported optically active materials with CTC in present study.

Previous study	Reference
Tris (diary amino)-triazine derivatives have good optical activity but are polycrystalline.	[9]
Triazine polymers contain Si and S atoms have high triplet band gap 2.91 eV and glass temperature (Tg) 148 °C.	[30]
Red orange emitter, 8-OH-quinolinolato Lithium.	[31]
Carbazole-triazine, Tg 165 °C, triplet energy 2.63 eV.	[32]
Star-shaped polymers (hindered extended pi-conjugation increased triplet energies to 2.80 eV and limited absorption of IR radiation.	[33]
Optically active benzidine-polyamide, ϵ 5.4 × 10^4, λ^{max}. 357 nm	[34]
Simple CTC, E_{CT} (2.899 eV-3.316 eV) optically active for fabrications laser lamps and photovoltaic cells.	[present study]

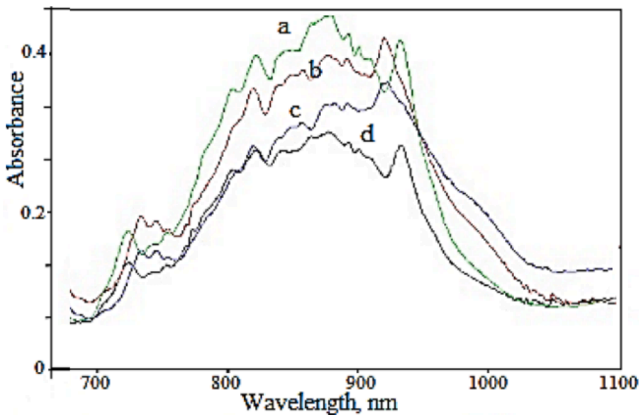

Fig. 4. Vibrational absorption of [(D1)(A1)] depoisted as thin film on Al foil at different temperature °C: a) 25, b) 30, c) 35, d) 40.

H^+ donation to vacant orbitals of es-donor atom *via* nπ* transition. Electronic UV-absorption spectra of CTC exhibit one CT band at 260–420 nm range, E_{CT}: 4.77–2.96 eV. This band at higher energies compared to CTC without H^+ transfer. This finding results from higher ionization potential of protonated Schiff bases molecule and lower electron affinity of anion A moleclue compared to neutral molecules [18].Small bands shift in D spectra attributed to *CT*-interactions at 397 nm, E_{CT} 3.132 eV for [(D1)(A2)]. For [(D1) $(A2)_2$], two bands at 375 nm, 429 nm, E_{CT} 3.316 eV, 2.899 eV clarified formation of CTC molecules. These intense electronic absorption bands are in good agreement with some reported CTC [18].

Long absorbance wavelength reflected good electron motilities of CTC as organic fluorescent heterocyclic chromospheres enabled uses in: molecular probes, fluorescent markers, Organic light-emitting diodes, photovoltaic cells and traditional textile and polymer fields. Electron donor's ability caused by electron mobility of D1, D2 in CTC are higher than that of polymers contain tri-, di-Ph.- NH_2-triazines and carbazoles [8]. Molar extension coefficient (ϵ $M^{-1}cm^{-1}$ $\times 10^4$] for [(D1)(A2)2], [(D2)(A2)], [(D2)(A2)2] are 12.6, 13.0, and 13.41 respectively reflect excellent optical properties in comparison to various polyamides (ϵ, 133.5) prepared with tedious synthetic routs using various toxic chemicals, λ^{max} 267, 305, 350, 413 nm [24].

The lowest energy electronic transition in CTC corresponds to es transfer from highest occupied molecular orbital (HOMO) $_{donor}$ to lowest vacant molecular orbital of acceptor (LUMO $_{acceptor}$). Excited electron at $(HOMO)_{donor}$ energy level give CT absorption UV-bands that may obscured by absorption bands of free D and A. [(D1)(A1)] is the most optically active CTC in terms of band intensity and numbers [18].

Stoichiometries of CTC are determined by using molar ratio spectrophotometric titrations [26]. Plot A:D ratio versus UV–vis. absorbance of characteristic absorption bands, Fig. 2 and Table 3.

Concentration of D (C_d^o) and A(C_A^o) are listed in Table 3.

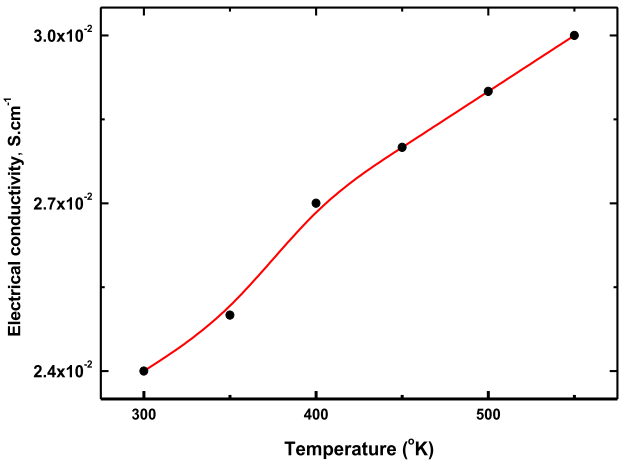

Fig. 5. Variation electrical conductivity of [(D1)(A1)] with temperature.

K_f of CTC are determined from plot represented in Fig. 3.

For D-A interaction in 1:1 or 1:2 M ratio:[(D1)(A1)], [(D1)$(A1)_2$] [(D1)(A2)] for [(D2)$(A2)_2$]. Stoichiometries agreed with elemental analysis [29]. These optically active CTC could be applied in manufacturing high internal efficiency organic light-emitting diodes (OLEDs) rather than using fluorescent emission polymers and dyes [27]. Table 4 showed comparative results of our study with other reported advanced optically active materials:

CTC [(D1)(A1)] deposited by cladding as thin film on sheet of aluminium (Al) foil showed good absorbance of IR radiation, Fig. 4.

Good absorbance of CTC to IR radiations at wavelength range (700–1000) nm confirmed CTC can thermal IR energy results from global warming and mitigate climate change by shielding IR radiation. Red shift $\lambda_{\cdot}^{max}$ reflected decrease band gap, Eg [28]. Absorbance at long $\lambda_{\cdot}^{max}$ 900–1100 nm in IR region indicating absorbance of thermal IR energy. Phonon bands at 900 nm originates from vibrational modes of harmonic and anharmonic oscillators in crystal lattice of CTC. Absorbed IR radiation causing thermal vibrations of atoms or molecules creating thermal phonons waves propagating in crystals lattice dissipating thermal IR energy [29].

Fig. 5 showed electrical conductivity of CTC [(D1)(A1)] is increased on heating as a typical semiconductor behavior due to thermally activated charge carriers' mobility [30].

Increasing AC electrical conductivity with rising temperature indicating electricity generation on heating that change intrinsic magnetic moments and permittivity; Phase change from non-polar *para*-electric phase to polar ferroelectric polar phase at Curie temperature, T_C [25] enables efficient energy storage.

CTC [(D1)(A1)] showed no thermal decomposition at T_C act as polar crystals can be used as tiny small sensors in electronic power generators converting chaotic waste heat into useful electric work. Polar crystals store electrical energy after removal of applied electric field and act as charge-reservoirs parallel plate electrical double layer capacitor. Piezoelectric CTC can be applied in automobiles electronics, touch screens of Lab top and mobile phones, as microwave filters and energy storage systems [25].

Under applied electric field, atomic electron clouds in polar crystals polarize. Dielectric constant and light refractive index depend on frequency of absorbed UV–vis. photons have quantized energy,*nhw*. Response of dielectric materials to electric field (E) is controlled by dielectric constant and AC conductivity that measures macroscopic dielectric properties and polarization. Dielectric materials are applied to capacitors, insulators and semiconductors. Ferroelectric dielectric perovskite crystals undergo phase change depending on heating or stress pressure at T_C, applied as electrostrictive actuators due to strong, electronic, power generation and saving [31]. [(D1)(A1)] has high nonlinear

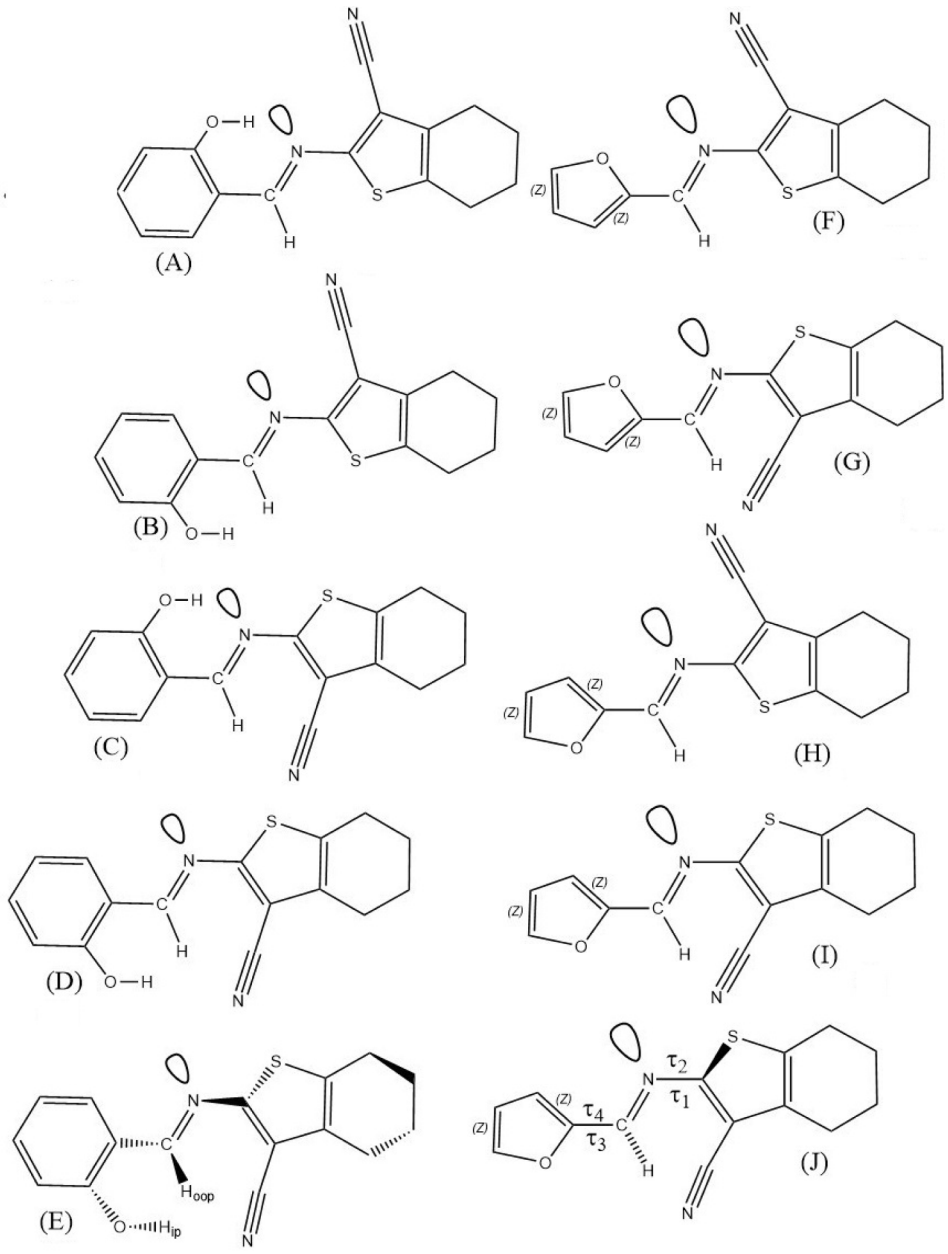

Fig. 6. Proposed structure: D1 (A-E), D2 (F-J).

optical (NLO) and good ferroelectric properties [8] for using in: infrared detectors, harvesting exhausted waste combustion heat from (pipe, automobiles batteries furnaces and chimneys to electricity [25].

Metal oxides ABO_3 perovskites: are pillar in electronics and nanotechnology as superconductive electrodes, magnetic, insulators, etc.; have cubic or semi-cubic crystalline structure. Ferroelectric piezoelectric low cost of promising lead-based perovskites. However Pb is toxic element [12]. Phases bithmus-, and barium- titanate, alkali Li, Na, K niobates NbO_3, bismuth- alkali titanates ($(Na_{0.5}Bi_{1/2})TiO_3$ and ($K_{0.5}Bi_{0.5}TiO_3$) as well as their solid solutions ((Ba, Ca)(Ti, Zr)O_3, ($Na_{0.5}Bi_{0.5}$)TiO_3-$BaTiO_3$ have no absorbance for thermal IR radiation [25].

CTC on Al foil can attain ferroelectric and magnetism in a single phase as good alternative to conventional materials such as $BiFeO_3$, $BiMnO_3$ and FeO_3, $LaFeO_3$. Polar semi organic CTC can attain improved anti-ferro-electricity, piezoelectricity, insulating behavior, semi conductivity, thermal stability, electrical conductivity, superconductivity, ferromagnetism, and anti-ferromagnetism, etc. [32].

Ab initio quantum Mechanics computational quantum chemistry confirmed molecular geometry for synthesized Schiff Ds using HyperChem Professional software program using basis set 6-31G*. Optimized geometries are shown in Fig. 6. *via* construction Cartesian coordinate matrix. In D1, C≡N moiety is *cis* towards lone-pair es of N atom (N_{LP}). OH is either *cis*, *Trans* to N_{LP} giving structure A and B respectively. Assigned *Trans* position of CH group, OH is directed cis and Trans against (N_{LP}) giving structure C, D respectively. These suggested non optimized hypotheticals retained the same proposed geometry. All suggested structures were flipped to non-planar optimized structure E with real vibrational frequencies where OH found OOP and C≡N moieties are *Trans* to N_{LP}. Dihedral angles $C_{11}C_{10}O_{14}H_{25}$ 24.1° and $C_{10}C_{11}C_7H_{15}$ equals 19.5° where low steric effects are conditioned since H_{25}, H_{15} are in- and out-of-plane respectively. Benzene and thiophene rings differ in planarity angles $C_{11}C_7N_6C_5$, $C_7N_6C_5C_2$ and $C_7N_6C_5S_4$ are optimized at −7.9°, −35.3° and −28.8°, respectively. Energy −1201a.u, dipole moment 3.225 Debye.

Similar computational outcomes were observed for compound D2.

Table 5
Comparative CTC in previous studies to thiophene-picric acid CTC in the current study.

CTC	Application	Ref.
Chloranilic acid-p-NO_2-aniline	Chemical and biology	[33]
1, 2-di.CH_3-limidazole-2, 4-di- NO_2-1-naphtho	Optical activity	[34]
o-phenylenediamine-PA	Academic research	[35]
8-aminoquinoline-chloranilic acid	Fluorescence emission	[36]
2-OH-pyridine-oxalic acid	Academic research	[37]

Cartesian coordinate matrix were constructed where O_{furan}, and C≡N moieties *cis* against N_{LP}. These two hypotheticals build up structures never been optimized retaining the same proposed geometry. Both suggested structures were flipped with two above mentioned moieties *trans* to N_{LP} avoiding 2D planarity of furan and thiophene rings which is little bit diagonal upon complete optimization with real vibrational frequencies in case of structure-J.

For D2molecule, O_9….H_{11} of 2.53 Å is less than 2.72 Å (sum Van der walls radii of O, and H atoms) favoring intra-molecular H. bonding as furan ring being telted by angle 1.2° ($\tau O_9C_8C_7H_{11}$) retaining quasi- 2D rearrangement compared to 19.5° analogues ($\tau C_{10}C_{11}C_7H_{15}$; D1). Furan and thiophene rings are in different planes. Dihedral angles 23.6°, 19.9° for τ_1CNCC and τ_2CNCS, respectively. Dihedral analogues in D1 $C_7N_6C_5C_2$ (-35.3°), $C_7N_6C_5S_4$ (28.8°) ensures non-planar benzene and furan rings against thiophene ring. Energy −1123.58793249 a.u. and dipole moment 2.766 Debye. Interatomic bond distances N19…*H*11 (2.82 Å) and N6….H30 (3.00 Å) indicate absence of H. Bonding. Weak intra-molecular H.B were predicted for S4….H21 (3.01 Å). HB however it is absent between S4….H22 (3.23) because it is larger than 3.00 Å [ ].

Our study added new to the application of CTC as explored in Table 5.

4. Conclusion

The prepared CTC has low charge transfer energy: 2.899 eV-3.316 eV indicated excellent optical activity and application as candidates coating materials in fabrications photovoltaic solar cells for saving and conserving solar energy, and laser lamps. Based on high molar extinction coefficients (ϵ, $M^{-1}cm^{-1}$, ($\times 10^3$]) of the prepared CTC up to 133.400. CTC are suitable light-emitting materials of unique optical and redox characteristics. Deposition CTC as thin film (TF) on aluminium foil decreased energy band gap for [D1A1] enhanced absorption of weak thermal IR photons to mitigate thermal heat. High thermal conductivity of CTC in the range 1.1 W.min-1.K-1–1.6 W.min-1.K-1 enabled attenuation of electromagnetic radiation and heat dissipation. Ab initio calculation confirmed dielectric properties and polarity of CTC that are IR active for attenuation thermal weak infra-red electromagnetic radiation.

Declaration of Competing Interest

The authors declare that they have no known competing financial interests or personal relationships that could have appeared to influence the work reported in this paper.

Data availability

Data will be made available on request.

Appendix A. Supplementary data

Supplementary data to this article can be found online at https://doi.org/10.1016/j.inoche.2023.110648.

References

[1] V. Coropceanu, X.K. Chen, T. Wang, Z. Zheng, J.L. Brédas, Charge-transfer electronic states in organic solar cells, Nat. Rev. Mater. 4 (11) (2019) 689–707.
[2] P. Srimuk, X. Su, J. Yoon, D. Aurbach, V. Presser, Charge-transfer materials for electrochemical water desalination, ion separation and the recovery of elements, Nat. Rev. Mater. 5 (7) (2020) 517–538.
[3] K.V. Karthik, A.V. Raghu, K.R. Reddy, R. Ravishankar, M. Sangeeta, N.P. Shetti, C. V. Reddy, Green synthesis of Cu-doped ZnO nanoparticles and its application for the photocatalytic degradation of hazardous organic pollutants, Chemosphere 1 (287) (2022 Jan), 132081.
[4] D. Yang, D. Ma, Development of organic semiconductor photodetectors: from mechanism to applications, Adv. Opt. Mater. 7 (1) (2019) 1800522.
[5] C. Bao, J. Yang, S. Bai, W. Xu, Z. Yan, Q. Xu, J. Liu, W. Zhang, F. Gao, High performance and stable all-inorganic metal halide perovskite-based photodetectors for optical communication applications, Adv. Mater. 30 (38) (2018) 1803422.
[6] M. Xiao, M.D. Shawkey, A. Dhinojwala, Bioinspired melanin-based optically active materials, Adv. Opt. Mater. 8 (19) (2020) 2000932.
[7] A. Kot, M. Radecka, D. Dorosz, K. Zakrzewska, Optically active TiO2: Er thin films deposited by magnetron sputtering, Materials 14 (15) (2021) 4085.
[8] T. Petit, L. Puskar, FTIR spectroscopy of nanodiamonds: Methods and interpretation, Diam. Relat. Mater. 89 (2018) 52–66.
[9] S.A. Shah, S. Baldelli, Chemical imaging of surfaces with sum frequency generation vibrational spectroscopy, Acc. Chem. Res. 53 (6) (2020) 1139–1150.
[10] K.Y. Su, W.L. Lee, Fourier transform infrared spectroscopy as a cancer screening and diagnostic tool: A review and prospects, Cancers 12 (1) (2020) 115.
[11] D. Maity, Biological Applications of Schiff base Metal Complexes-A Review, International Journal of Research and Analytical Reviews 6 (2) (2019) 471–478.
[12] V. Alagarsamy, K. Chitra, G. Saravanan, V.R. Solomon, M.T. Sulthana, B. Narendhar, An overview of quinazolines: Pharmacological significance and recent developments, Eur. J. Med. Chem. 151 (2018) 628–685.
[13] S. Amirat, F. Madi, M. Bououdina, A. Gheid, A. Zaboub, L. Nouar, R. Merdes, Computational study on intermolecular charge transfer complex of 2, 2′-bipyridine with picric acid: TD-DFT, NBO and QTAIM analysis, Mater. Res. Express 6 (7) (2019), 075104.
[14] Flores, V.C., Keyzer, H., Varkey-Johnson, C. and Young, K.L., 2022. Related Topics I: Charge-Transfer Complexes in Biological Systems. In *Organic Conductors* (pp. 691-734). CRC Press.
[15] J.A. Ruiz-Arias, C.A. Gueymard, Worldwide inter-comparison of clear-sky solar radiation models: Consensus-based review of direct and global irradiance components simulated at the earth surface, Sol. Energy 168 (2018) 10–29.
[16] H. Luo, A. Gravouil, V. Giordano, A. Tanguy, Thermal transport in a 2D nanophononic solid: Role of bi-phasic materials properties on acoustic attenuation and thermal diffusivity, Nanomaterials 9 (10) (2019) 1471.
[17] H.A. Fetouh, H. Abdel-Hamid, A.A.H. Zaghloul, A.E. Ghadban, A.M. Ismail, Formulation of promising antibacterial, anticancer, biocompatible and bioactive biomaterial as therapeutic drug delivery system for biologically active compound loaded on clay polymer, Polymer Bulletin (2022) 1–25.
[18] E.H. El-Mossalamy, M.E. Batouti, H.A. Fetouh, The role of natural biological macromolecules: Deoxyribonucleic and ribonucleic acids in the formulation of new stable charge transfer complexes of thiophene Schiff bases for various life applications, Int. J. Biol. Macromol. 193 (2021) 1572–1586.
[19] J.S. McIndoe, K.L. Vikse, Assigning the ESI mass spectra of organometallic and coordination compounds, J. Mass Spectrom. 54 (5) (2019) 466–479.
[20] A. Novais, A.R. Freitas, C. Rodrigues, L. Peixe, Fourier transform infrared spectroscopy: unlocking fundamentals and prospects for bacterial strain typing, Eur. J. Clin. Microbiol. Infect. Dis. 38 (3) (2019) 427–448.
[21] S.A. Khan, S.B. Khan, L.U. Khan, A. Farooq, K. Akhtar, A.M. Asiri, Fourier transform infrared spectroscopy: fundamentals and application in functional groups and nanomaterials characterization. In *Handbook of materials characterization*, Springer, Cham, 2018, pp. 317–344.
[22] N. Badi, S. Khasim, A. Pasha, A.S. Alatawi, M. Lakshmi, Silver nanoparticles intercalated polyaniline composites for high electrochemical anti-corrosion performance in 6061 aluminum alloy-based solar energy frameworks, Journal of Bio-and Tribo-Corrosion 6 (4) (2020) 1–9.
[23] M. El Batouti, H.A. Fetouh, A facile new modified method for the preparation of a new cerium-doped lanthanium cuperate perovskite energy storage system using nanotechnology, New J. Chem. 45 (19) (2021) 8506–8515.
[24] A. Kamimura, K. Ikeda, Y. Akinari, H. Matsumoto, K. Kaiso, A study on the stereochemistry of direct conversion of polyamides to hydroxyesters using monomeric secondary chiral amines as a model compound, Polym. Degrad. Stab. 160 (2019) 162–167.
[25] R.S. Almufarij, A.E. Ali, M.E. Elbah, N.S. Elmaghraby, M.A. Khashaba, H. Abdel-Hamid, H.A. Fetouh, Preparation, Characterization of New Antimicrobial Antitumor Hybrid Semi-Organic Single Crystals of Proline Amino Acid Doped by Silver Nanoparticles, Biomedicines 11 (2) (2023) 360.
[26] V. Abbu, V. Nampally, N. Baindla, P. Tigulla, Stoichiometric, thermodynamic and computational DFT analysis of charge transfer complex of 1-benzoylpiperazine with 2, 3-dichloro-5, 6-dicyano-1, 4-benzoquinone, J. Solution Chem. 48 (1) (2019) 61–81.
[27] W. Song, Q. Xu, J. Zhu, Y. Chen, H. Mu, J. Huang, J. Su, Imidazo [1, 2-b] pyridazine as building blocks for host materials for high-performance red-phosphorescent organic light-emitting devices, ACS Appl. Mater. Interfaces 12 (17) (2020) 19701–19709.
[28] Liu, C., Alam, M.Z., Pang, K., Manukyan, K., Hendrickson, J.R., Smith, E.M., Zhou, Y., Reshef, O., Song, H., Zhang, R. and Song, H., 2020, May. Experimental

demonstration of self-phase-modulation induced wavelength shift in an 80-nm thick ITO-ENZ material in the telecom C band. In *CLEO: QELS_Fundamental Science* (pp. FTu3Q-5). Optical Society of America.

[29] J. Cunha, T.L. Guo, G. Della Valle, A.N. Koya, R. Proietti Zaccaria, A. Alabastri, Controlling light, heat, and vibrations in plasmonics and phononics, Adv. Opt. Mater. 8 (24) (2020) 2001225.

[30] S. Hettler, D. Sebastian, M. Pelaez-Fernandez, A.M. Benito, W.K. Maser, R. Arenal, In-situ reduction by Joule heating and measurement of electrical conductivity of graphene oxide in a transmission electron microscope, 2D Materials 8 (3) (2021), 031001.

[31] O.M. Mailoud, A.H. Elsayed, A.H. Abo-Elazm, H.A. Fetouh, Synthesis and study the structure, optical, thermal and dielectric properties of promising Glycine Copper Nitrate (GCN) single crystals, Results Phys. 10 (2018) 512–520.

[32] Yanchevskii, O.Z., V'yunov, O.I., Belous, A.G. and Kovalenko, L.L., 2021. Dielectric properties of CaCu3Ti4O12 ceramics doped with aluminium and fluorine. *Journal of Alloys and Compounds*, *874*, p.159861.

[33] I.M. Khan, A. Ahmad, L. Miyan, M. Ahmad, N. Azizc, Synthesis of charge transfer complex of chloranilic acid as acceptor with p-nitroaniline as donor: Crystallographic, UV–visible spectrophotometric and antimicrobial studies, J. Mol. Struct. 1141 (2017) 687–697.

[34] L. Miyan, I.M. Khan, A. Ahmad, Synthesis, and spectroscopic studies of charge transfer complex of 1, 2-dimethylimidazole as an electron donor with π-acceptor 2, 4-dinitro-1-naphthol in different polar solvents, Spectrochim. Acta A Mol. Biomol. Spectrosc. 146 (2015) 240–248.

[35] I.M. Khan, A. Ahmad, Synthesis, spectral and thermal studies of the newly hydrogen bonded charge transfer complex of o-phenylenediamine with π acceptor picric acid, Spectrochim. Acta A Mol. Biomol. Spectrosc. 77 (2) (2010) 437–441.

[36] I.M. Khan, M. Islam, S. Shakya, N. Alam, S. Imtiaz, M.R. Islam, Synthesis, spectroscopic characterization, antimicrobial activity, molecular docking and DFT studies of proton transfer (H-bonded) complex of 8-aminoquinoline (donor) with chloranilic acid (acceptor), J. Biomol. Struct. Dyn. 40 (22) (2022) 12194–12208.

[37] I.M. Khan, S. Shakya, R. Akhtar, K. Alam, M. Islam, N. Alam, Exploring interaction dynamics of designed organic cocrystal charge transfer complex of 2-hydroxypyridine and oxalic acid with human serum albumin: Single crystal, spectrophotometric, theoretical and antimicrobial studies, Bioorg. Chem. 100 (2020), 103872.